PAPER

Check for updates

Solution-processed broadband photodetectors without transparent conductive oxide electrodes

Lening Sheng,†[a] Chao Yi,†[a] Luyao Zheng,†[a] Yanghe Liu,[a] Jie Zheng [iD][b] and Xiong Gong [iD] *[a]

Broadband photodetectors (PDs) have great applications in both industrial and scientific sectors. In this study, solution-processed broadband PDs with an "inverted" vertical photodiode device structure without incorporating transparent conductive oxides electrodes, fabricated by bulk heterojunction (BHJ) composites composed of a low optical gap conjugated polymer blended with highly electrically conductive PbS quantum dots (QDs), operated at room temperature, are reported. The low optical gap conjugated polymer incorporated with PbS QDs contributes to the spectral response from the ultraviolet (UV)-visible to the infrared (IR) range. To realize the IR spectral response and to circumvent the weak IR transparency of the transparent oxide electrodes, the implementation of a photodiode with an "inverted" vertical device structure with the Au anode and the Ba/Al bilayer semitransparent cathode passivated with the MgF$_2$ layer is demonstrated. Photoinduced charge carrier transfer occurring within the BHJ composite gave rise to decent photocurrent, resulting in detectivities greater than 10^{12} Jones (cm Hz$^{1/2}$/W) over the wavelength from the UV-visible to the IR range under low applied bias. Thus, our findings of the utilization of the BHJ composites and an "inverted" vertical photodiode without the incorporation of the transparent conductive oxide electrodes provide a facile way to realize broadband PDs.

1. Introduction

Broadband photodetectors (PDs) have drawn great attention in both academic and industrial sectors due to their various applications including telecommunications, day/night surveillance, thermal imaging, chemical/biological sensing, and spectroscopic and medical instruments.[1–4] To realize broadband PDs, current PDs with different sub-bands were integrated to one electronic device to cover the spectral response from the ultraviolet (UV)-visible to the infrared (IR) range.[1–5] Moreover, InCaAs- and HgCdTe-based IR PDs require an extremely low operating temperature (4.2 K) and operate at high voltage to achieve reasonable detectivity.[1,2] In addition, expensive manufacturing processes are required to fabricate these IR PDs.[1–3,6] All these requirements restrict their application in biosensors and image sensors where both high sensitivity and low operating voltage are required.[1–3]

In the past years, inorganic quantum dot (QD)-based PDs with a planar device structure have been extensively studied to realize IR responsibility but high operation voltages were required to achieve a decent detectivity.[4,6–10] Two-dimensional (2D) materials, such as graphene and transition metal dichalcogenides, have been studied as alternatives to demonstrate IR detection with high detectivities through PDs with the same device structure as that of thin-film transistors (TFTs).[11–14] However, their applications are restricted by the difficulty in the large-scale and high throughput fabrication of mono and multilayer 2D materials as well as the high gate (or drive) voltages to be used for TFTs.[11–14] In the past two decades, organic/polymer-based PDs have gained abundant attention due to their advanced features such as ease of processing, low cost, physical flexibility, and excellent optoelectronic properties.[5,15–17] In 2009, we reported polymer-based PDs with a spectral response from 300 nm to 1450 nm.[5] Recently, we demonstrated polymer-based PDs with spectral response from 300 nm to 2500 nm.[17] Various novel molecules were developed for extending the spectral response of polymer-based PDs.[18–21] Furthermore, film morphology evolution,[22] interfacial engineerings,[23,24] molecular engineering and arrangement,[25,26] and the photomultiplication (PM) effect[27–29] have been used to enhance the detectivities of polymer-based PDs. However, it is still a challenge to realize polymer-based PDs with decent IR photoresponse because of their short exciton lifetime induced by phonon-exciton recombination.[30–34]

To circumvent the above challenges, either polymers or hybrid perovskites incorporated with inorganic QDs have been developed to realize broadband PDs.[4,23,24,35–41] In the past years, we have reported various room-temperature (RT) operated

[a] *School of Polymer Science and Polymer Engineering, The University of Akron, Akron, OH 44325, USA. E-mail: xgong@uakron.edu; Fax: (330) 972 3406*

[b] *Department of Chemical, Biomolecular and Corrosion Engineering, College of Engineering and Polymer Science, The University of Akron, Akron, OH 44325, USA*

† These authors contributed to this work equally.

This journal is © The Royal Society of Chemistry 2022

J. Mater. Chem. C, 2022, **10**, 2783–2791 | **2783**

broadband PDs by conjugated polymers, inorganic QDs, conjugated polymers incorporated with inorganic QDs, and hybrid perovskites incorporated with inorganic QDs.[4,23,24,35–41]

On the other hand, transparent electrodes are required to realize PDs with IR spectral response. However, currently widely used transparent conductive oxides, such as indium tin oxide (ITO) and fluorine-doped tin oxide (FTO), as the transparent electrodes for various electronics including sensors and PDs possess very weak transmittance in the IR region.[42–44] Thus, PDs with a planar device structure and a TFT device structure were developed to avoid using neither ITO nor FTO electrodes, thus realizing IR spectral response.[6–14] Furthermore, carbon nanotubes (CNTs),[45,46] silver nanowires (Ag NWs),[47] and semiconducting polymers[48–51] were under intensive investigation for the substitution of ITO or FTO electrodes. However, CNTs and Ag NWs thin films possess poor electrical conductivity[45–49] and were required to be processed with complicated costly nanoimprint lithography as well.[45–49] Semiconducting polymer thin films as transparent electrodes have drawn much attention owing to their advanced features such as low cost, lightweight, mechanical flexibility, and compatibility with plastic substrates.[50,51] But the semiconducting polymer thin film with high electrical conductivities needs to be treated with strong acids,[50,51] which restrict its practical applications in electronics. Recently, we demonstrated flexible solution-processed broadband PDs with a "vertical" sandwiched device structure, made by hybrid perovskites incorporated with PdSe QDs, based on the solution-processed polymeric thin film as the transparent electrode.[42]

In this study, we report room-temperature (RT) operated solution-processed broadband PDs fabricated by the bulk heterojunction (BHJ) composites composed of a low optical gap conjugated polymer blended with highly electrically conductive PbS QDs and with an "inverted" vertical photodiode device structure without incorporating the transparent conductive oxide electrodes. The low optical gap conjugated polymer contributes to the IR photoresponse up to 1700 nm. PbS QDs further extend the IR photoresponse up to 2000 nm. To realize IR spectral response and circumvent the weak IR transparency of the transparent oxides' electrodes, the implementation of a photodiode with an "inverted" vertical device structure with the Au anode and the Ba/Al bilayer semitransparent cathode passivated with the MgF$_2$ layer, is demonstrated. Photoinduced charge carrier transfer occurring within the PDDTT:PbS QDs BHJ composite gave rise to decent photocurrent, resulting in detectivities greater than 10^{12} Jones (cm Hz$^{1/2}$/W) over the wavelength region from 300 nm to 2000 nm under low applied bias. Thus, our findings of the utilization of the PDDTT:PbS QDs BHJ composites and an "inverted" vertical photodiode without incorporation with the transparent oxide electrodes provide a facile way to realize broadband PDs.

2. Experimental section

2.1. Materials

PbO (99.999%) was purchased from Alfa Aesar. Oleylamine (OLA) (90%), 1-octadecene (ODE) (90%), trioctylphosphine (TOP) (97%), diphenylphosphine (DPP) (98%), selenium (99.99%), 1,2-ethanedithiol (EDT) (98%), methanol (99.8), and acetonitrile (ACN) (99.8%) were purchased from Sigma Aldrich. All materials were used as received without further purification. PDDTT was synthesized in our lab following the procedures reported previously.[5]

Synthesis of PbS QDs. PbCl$_2$ (1 mmol, 0.28 g) was added to 5 mL of oleylamine (OLA) at RT, and then heated to 120 °C under vacuum and stirred vigorously until the PbCl$_2$-OLA mixture turned into a homogeneous clear solution. Elemental sulfur (0.4 mmol, 14 mg) was dissolved in 2.5 mL of OLA by heating at 80 °C in an oil bath, which gave a deep red solution. The resultant sulfur solution was injected into the PbCl$_2$-OLA solution at 140 °C, and then kept for 1 hour. The resultant solution was further centrifuged and purified to generate OLA-capped PbS QDs power. The OLA-capped PbS QDs thin film was spin-cast from the 50 mg mL^{-1} OLA-capped PbS QDs octane solution, and the cast EDT acetonitrile solution on the top of the OLA-capped PbS QDs. Afterward, acetonitrile solvent was used to wash out the excess organic ligand. The above steps were repeated several times for obtaining the EDT-capped PbS QDs thin film.

2.2. Preparation and characterization of thin films

PDDTT and PbS QDs thin films, and PDDTT:PbS QDs BHJ composite thin film were fabricated through the spin-coating method from their corresponding solutions. The absorption spectra of the thin films were measured by a Lambda 750 UV/Vis/NIR spectrometer from PerkinElmer. The transmission electron microscopy (TEM) images were measured using a Model JEOL JSM-1230. The thin film thickness was measured on the DektakXT surface profile system. The transient absorption measurements were carried out using a dual-beam femtosecond spectrometer utilizing the second harmonic of an OPA (optical parametric amplifier) as the pump and a white light continuum as the probe in Professor Alan J. Heeger's laboratory at the University of California, Santa Barbara.

Fabrication and characterization of TFTs. The "bottom-contact" TFTs device structure was treated in hexamethyldisilazane before the deposition of the PbS QDs thin films. The TFTs device structures with different source-drain separations were fabricated on an n-doped Si wafer; the n-doped Si was used as the gate. The gate dielectric was a 200 nm film of SiO$_2$ thermally grown directly on the wafer. The source and drain electrodes (Au) were deposited on SiO$_2$ by e-beam evaporation. The channel lengths (source-drain separation) were 25 μm and the channel width was 1000 μm. Electrical measurements were carried out using a Keithley 4200 Semiconductor Characterization System in ambient conditions.

2.3. Fabrication and characterization of broadband PDs

Commercially available Au/Cr caped on the glass substrates were cleaned with deionized water, acetone, and isopropanol and then dried out in vacuum overnight. After UV ozone plasma treatment for 20 min (mins) in ambient atmosphere, ∼30 nm MoO$_3$ layer was deposited on the top of the Au/Cr surface by the

2784 | *J. Mater. Chem. C*, 2022, **10**, 2783–2791

This journal is © The Royal Society of Chemistry 2022

spin-coating method from the MoO_3 precursor solution, followed by thermal annealing at 120 °C for 30 min. ~ 200 nm PDDTT:PbS QDs BHJ composite thin film was spin-coated on the top of the MoO_3 layer from the PDDTT:PbS QDs BHJ composite toluene solution. After that, ~ 10 nm BaO, ~ 5 nm Ba, ~ 20 nm Al, and ~ 400 nm MgF_2 were thermally deposited consequently through a shadow mask under 1×10^{-6} mbar vacuum. The device area was measured to be 0.16 cm^2.

The current density–voltage (J–V) characteristics of broadband PDs were obtained using a Keithley model 2400 source measurement unit. A Newport Air Mass 1.5 Global (AM1.5G) full-spectrum solar simulator was applied as the light source. The light intensities for the wavelength (λ) of 800 nm was 0.22 mW cm^{-2} and for λ = 1550 nm was 0.05 mW cm^{-2}. The external quantum efficiency (EQE) spectra were measured by a quantum efficiency measurement system (QEX10) with a 300 W steady-state xenon lamp as the source light. Transient photocurrent measurement was performed on a homemade setup using an optical chopper controlled using λ = 532 nm laser pulse at a frequency of 2 kHz.

3. Results and discussion

To enhance the electrical conductivity of PbS QDs, 1,2-ethanedithiol (EDT), which has a short thiol (S–H) chain, is used to substitute OLA, which has a long carbon chain (C–C), through the ligand exchange process,[52–55] for generating the EDT-capped PbS QDs (termed as EDT-PbS QDs). After that, the EDT-capped PbS QDs were rinsed with CH_3OH and then treated with $NH_3 \cdot H_2O$, followed by thermal annealing at 150 °C for 10 min. The molecular structures of OLA and EDT are shown in Fig. 1a. The TEM images of the OLA-capped PbS QDs and EDT-capped PbS QDs thin films are presented in Fig. 1b and c.

Based on the TEM image, the average particle size of the OLA-capped PbS QDs is estimated to be ~ 9 nm, whereas the average particle size of the EDT-capped PbS QDs is estimated to be ~ 12 nm. Thus, the treatment described above could enlarge the particle size of the PbS QDs.

Fig. 1d presents the absorption spectra of PbS QDs. The absorption of the OLA-capped PbS QDs is extended to 1900 nm, whereas the absorption of the EDT-capped PbS QDs is extended to 2100 nm. Thus, the optical bandgap (E_g) is estimated to be 0.65 eV for the OLA-capped PbS QDs thin film and 0.59 eV for the EDT-capped PbS QDs thin film. According to the quantum confinement effect,[56] the particle size of the OLA-capped PbS QDs is estimated to be ~ 9 nm, whereas the particle size of the EDT-capped PbS QDs is estimated to be ~ 13 nm. These results are in good agreement with the TEM images (Fig. 1b and c).

To verify the hypothesis that the EDT-capped PbS QDs thin film possess superior electronic properties than that of the OLA-capped PbS QDs, the TFTs are applied to study the field-effect mobilities of the two different PbS QDs thin films. The field-effect mobility in the saturation regime was extracted using the equation $I_{DS} = C_i \mu (V_{GS} - V_{Th})^2 W/2L$,[57] under the condition of $-V_{DS} > -(V_{GS} - V_{Th})$, where I_{DS} is the source/drain current, μ is the field-effect mobility, W is the channel width, L is the channel length, C_i is the capacitance per unit area of the gate dielectric layer, and V_{GS}, V_{Th}, and V_{DS} are the gate, threshold, and source/drain voltages, respectively. Fig. 2a presents the I_{DS} *vs.* V_G characteristics of the TFTs made using two different PbS QDs thin films. The field-effect mobilities of $\sim 1 \times 10^{-5}$ cm^2 V^{-1} s^{-1} and $\sim 2.2 \times 10^{-3}$ cm^2 V^{-1} s^{-1} are observed from the OLA-capped PbS QDs thin film and the EDT-capped PbS QDs thin film, respectively. The field-effect hole mobility of the EDT-capped PbS QDs thin film is ~ 100 times larger than that of the OLA-capped PbS QDs thin film.

Fig. 1 (a) Molecular structures of OLA and EDT, the TEM images of (b) the OLA-capped PbS QDs thin film and (c) the EDT-capped PbS QDs thin film, and (d) the absorption spectra of two different PbS QDs thin films.
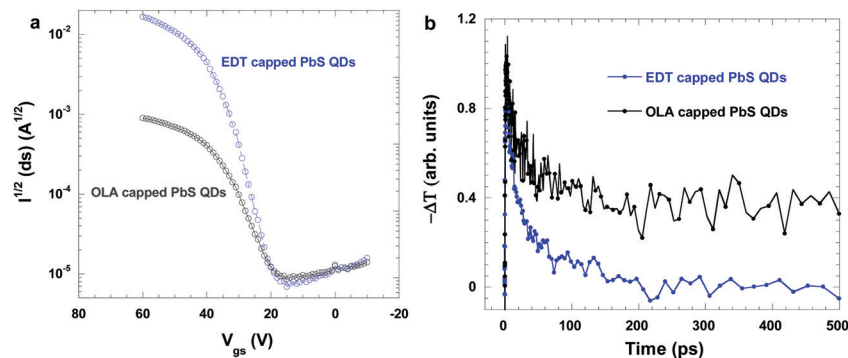
Fig. 2 (a) The I_{DS} versus V_G characteristics of thin-film transistors based on the PbS QDs thin films, (b) the transient decay dynamics of PbS QDs thin films probed at 4.7 mm.

The enhanced charge carrier mobility of the EDT-capped PbS QDs thin film is ascribed to the short-chain of the EDT molecule.

Fig. 2b compares the dynamics of the photoinduced absorption in the OLA-capped PbS QDs thin film and the EDT-capped PbS QDs thin film probed at 4.7 mm. Compared to the OLA-capped PbS QDs, a fast decay from the EDT-capped PbS QDs thin film was observed. A slow decay indicates that the traps induced by the insulating OLA restrict electron hopping from one PbS QD to another. On the other hand, a fast decay observed from the EDT-capped PbS QDs reveals that the electron can hop from one PbS QDs to another with less restriction. These results demonstrate that the charge carrier mobility of the EDT-capped PbS QDs is higher than those of the OLA-capped PbS QDs.

Fig. 3a presents the molecular structures of PDDTT with different side chains, where PDDTT is poly(5,7-bis(4-decanyl-2-thienyl)-thieno(3,4-b)diathiazole-thiophene-2,5). PDDTT is selected as the electron donor to form the bulk heterojunction (BHJ) composite with PbS QDs since it has a p-type low optical gap-conjugated polymer with decent charge carrier mobility.[5] Moreover, PDDTT exhibits optical response up to the near-infrared (NIR) region, which could certainly contribute to the NIR spectral response for broadband PDs based on PDDTT composites.[5] However, PDDTT with $C_{10}H_{21}$ side chain (PDDTT-C10) possesses poor solubility in typical organic solvents.

To enhance its solubility, a side chain with a long carbon chain, such as $C_{12}H_{25}$ was incorporated with PDDTT. The synthetic procedures of PDDTT with the $C_{12}H_{25}$ side chain (PDDTT-C12) were the same as PDDTT-C10, which was reported previously.[5,58] The absorption spectra of the PDDTT-C10 and PDDTT-C12 thin films are shown in Fig. 3b. Due to polymer aggregation,[59] PDDTT-C12 thin film possesses extended absorption compared to the PDDTT-C10 thin film. Thus, PDDTT-C12 was used as the electron donor to form a BHJ composite with the EDT-capped PbS QDs for the development of broadband PDs.

Scheme 1a displays the device architecture of the broadband PDs. In this broadband PDs, neither ITO nor FTO, which are currently used as the transparent electrodes for various electronics, are used as the electrodes due to their very weak transmittance in the IR region.[43-45] Moreover, carbon nanotubes (CNTs),[45,46] silver nanowires (Ag NWs),[47] and semiconducting polymers[48-51] were also not utilized as the transparent electrodes since they possess poor electrical conductivity and are required to be processed with complicated costly nanoimprint lithography.[45-49] Towards the end, an ''inverted'' device architecture, as shown in Scheme 1a, was developed. In this device structure, the Au/Cr bilayer is the anode, solution-processed MoO_3 thin layer acts as the hole extraction layer (HEL), the PDDTT:PbS QDs BHJ composite thin film is the photoactive layer, the vacuum-deposited BaO thin layer acts as the electron

Fig. 3 (a) Molecular structures and (b) absorption spectra of PDDTT with different side chains.
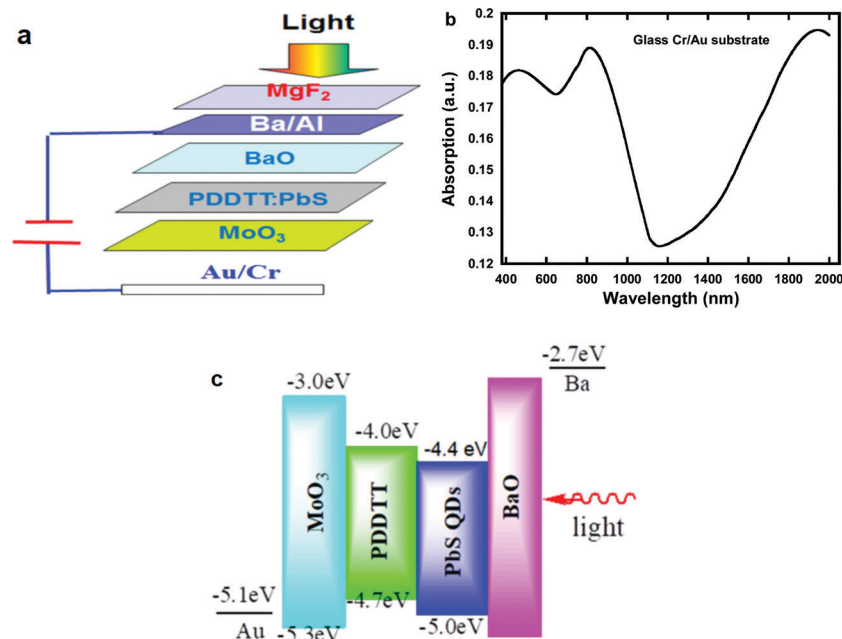
Scheme 1 (a) Device architecture of broadband photodetectors, (b) the absorption spectrum of glass Cr/Au thin film, and (c) the LUMO and HOMO energy levels of MoO_3, PDDTT, PbS QDs, BaO, and the work functions of the Au and Ba electrodes.

extraction layer (EEL), thin Ba covered with Al bilayer acts as the cathode, and the transparent MgF_2 layer is used as the passivation layer since it has excellent transparency from the UV-visible to the IR region.[60] The Ba/Al (5 nm/20 nm) bilayer has decent transparency from the UV-visible to the IR region as well.[61] BaO is a wide optical gap oxide. The light passing through the BaO EEL will be absorbed by the PDDTT:PbS QDs BHJ composite thin film. Moreover, smooth Au layer typical can reflect 30% of light.[62] Scheme 1b displays the absorption spectrum of the glass Cr/Au thin film. It is clear that the smooth Au thin layer could reflect light from 300 nm to 2000 nm. This reflected light can be further reabsorbed by the PDDTT:PbS QDs BHJ composite thin film, resulting in boosted photocurrent. As a result, a decent photocurrent is expected to be observed from the broadband PDs with a device structure shown in Scheme 1a.

Scheme 1c displays the lowest unoccupied molecular orbital (LUMO) and the highest occupied molecular orbital (HOMO) energy levels of MoO_3, PDDTT, PbS QDs, BaO, and the work-functions of the Au and Ba electrodes. Without illumination, the Schottky barrier formed between the Au anode and the MoO_3 HEL, and the Ba cathode and the BaO EEL could result in suppressed dark current density for broadband PDs. Under illumination, the excitons generated within the PDDTT:PbS QDs BHJ composite photoactive layer would dissociate into separated charge carriers under an external electric field created by the work function difference between the Au and Ba electrodes. Based on the band alignment, the separated electrons within the PDDTT:PbS QDs BHJ composite could transfer from PDDTT to PbS QDs due to a large LUMO offset between PDDTT and PbS QDs. These separated electrons are further extracted by the BaO HEL, and then collected by the Ba cathode. Meanwhile, the separated holes within the PDDTT:PbS QDs BHJ composite could transfer from PbS QDs

to PDDTT due to a large HOMOs offset between the PbS QDs and PDDTT. These separated holes are further extracted by the MoO_3 HEL, and then collected by the Au anode. Therefore, broadband PDs with a device structure shown in Fig. 1a would exhibit boosted R and D^*.[5]

To verify the photoinduced charger transfer occurring within the PDDTT:PbS QDs BHJ composite, the dynamics of the photoinduced absorption in the PDDTT:PbS QDs BHJ composite thin film probed at 4.7 μm is investigated and further compared with those of pristine PDDTT and PbS QDs. The polarons from the conjugated polymers could be detected in the mid-IR spectral region.[63–65] As indicated in Fig. 4a, a fast decay observed from the pristine PDDTT thin film indicates that the lifetime of the polarons from PDDTT is very short. A relatively slow decay observed from the EDT-capped PbS QDs indicates that the charge carrier is trapped due to the insulation of the EDT molecule. However, a much longer polaron lifetime, which is up to a nanosecond, is observed from the PDDTT:PbS QD BHJ composite thin film as compared to those from the pristine PDDTT thin film and the pristine PbS QD thin film. These results reveal that the long-lived mobile carriers show the integration of PDDTT and PbS QDs, and further demonstrate the efficient charge transfer from PDDTT to PbS QDs with inhibited back-transfer. Thus, as expected, broadband PDs based on the PDDTT:PbS QD BHJ composite thin film would exhibit high photocurrent.

The current density versus voltage (J–V) characteristics of broadband PDs operated at RT and measured in dark and under a monochromatic light at a wavelength (λ) of 800 nm with a light intensity of 0.22 mW cm^{-2}, and at a λ of 1550 nm with a light intensity of 0.05 mW cm^{-2}, are shown in Fig. 4b. In dark, the broadband PDs exhibit asymmetric J–V characteristics with the ratification ratio of 2.5×10^4 at ±1 V. These results indicate
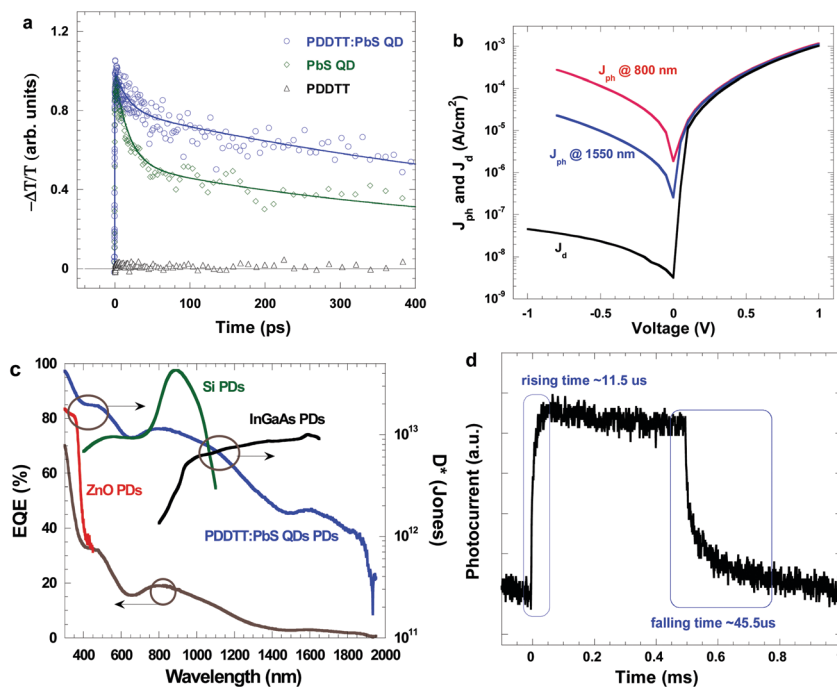
Fig. 4 (a) The transient decay dynamics of PDDTT and PbS QDs thin films and PDDTT:PbS QDs BHJ composite thin film, (b) the $J–V$ characteristics of broadband PDs, (c) the EQE spectrum of the broadband PDs and the projected detectivities of the broadband PDs *versus* wavelength compared with ZnO-based PDs, Si-based PDs, and InGaAs-based PDs, and (d) the photocurrent response time of broadband PDs.

that the broadband PDs possess excellent photodiode behaviors.[66] Different photocurrent densities observed from the broadband PDs under different monochromatic light illumination are ascribed to different light intensities, which indicate that the broadband PDs possess different photoresponsibilities.

Responsivity (R), described as $R = J_{ph}/L_{light}$[5,66] (where J_{ph} is the photocurrent density and L_{light} is the light intensity), is often used to evaluate the device performance of the PDs. Under a bias of -0.1 V, R of 73 mA W^{-1} and 28.8 mA W^{-1} at λ of 800 nm and 1550 nm, respectively, are observed from the broadband PDs. Moreover, under a bias of -0.5 V, R of 545 mA W^{-1} and 195 mA W^{-1} at λ of 800 nm and 1550 nm, respectively, are observed from the broadband PDs.

If the dark current is only considered as the major contributor to the noise current,[5,36,37] the project detectivity (D^*) can be described as $D^* = R/\sqrt{2qJ_d}$[5] (where J_d is the dark current density, q is the elementary electric charge, $q = 1.6 \times 10^{-19}$ C, respectively). Thus, at RT, D^* at λ of 800 nm and 1550 nm are calculated to be 1.6×10^{13} Jones and 6.4×10^{12} Jones (cm Hz$^{1/2}$/W), respectively, for the broadband PDs operated at a bias of -0.1 V. Moreover, at RT and under a bias of -0.5 V, D^* at λ of 800 nm and 1550 nm was calculated to be 1.2×10^{14} Jones and 4.3×10^{13} Jones, respectively, for broadband PDs. These D^* values are compatible with those observed from 2D metal dichalcogenide-based PDs.[11–14] All these results certainly demonstrate that broadband PDs with a vertical device structure exhibit high R and D^*, indicating that the broadband PDs have great potential applications.[1–3]

Fig. 4c presents the EQE spectrum of the broadband PDs. It is clear that the EQE spectrum of the broadband PDs is the superposition of the absorption spectra of the EDT-capped PbS QDs thin film (Fig. 1), PDDTT thin film (Fig. 3), and the reflection spectrum of the Au thin layer (Scheme 1b).

Based on the EQE spectrum and D^* value at λ of 800 nm and 1550 nm for the broadband PDs, D^* values *versus* wavelength are calculated based on $R = \text{EQE} \times \dfrac{q}{h\nu} = \text{EQE} \times \dfrac{\lambda}{1240}$.[5,66] Fig. 4c presents D^* *versus* wavelength for the broadband PDs. Under a bias of -0.1 V, the broadband PDs exhibit over 10^{12} Jones from 300 nm to 2000 nm at RT. Such decent D^* over the broadband spectral region are ascribed to novel device architecture and the PDDTT:PbS QDs BHJ composite thin film.

The response time is another important parameter used to evaluate the device performance of the PDs. Fig. 4d presents the transient photocurrents of the broadband PDs. The rise time was defined as the time required for the output signals to increase from 10% to 90% of the saturated photocurrent. Similarly, the fall time was defined as the time required for the output signal to decrease from 90% to 10% of the saturated photocurrent.[67,68] A rise time of 11 μs and a fall time of 45 μs was observed from the broadband PDs. Such slow response time is probably originated from the relatively poor electrical conductivity of the EDT-capped PbS QDs thin film.

4. Conclusion

Room-temperature operated, solution-processed broadband photodetectors (PDs) based on low optical gap conjugated polymer incorporated with highly electrically conductive PbS

2788 | *J. Mater. Chem. C*, 2022, **10**, 2783–2791

This journal is © The Royal Society of Chemistry 2022

quantum dots (QDs) bulk heterojunction (BHJ) composite and inverted photodiode device structure without the incorporation of the transparent oxide electrodes, with the spectral response ranging from 300 nm to 2000 nm, were demonstrated. The low optical gap conjugated polymer, PDDTT, contributes to the IR photoresponse up to 1700 nm. PbS QDs further extend the IR photoresponse up to 2000 nm. The implementation of a photodiode with an "inverted" vertical device structure with the Au anode and the Ba/Al bilayer semitransparent cathode passivated with the MgF$_2$ layer realize IR spectral response and circumvent the weak IR transparency of the transparent oxide electrodes. Photoinduced charge carrier transfer within the PDDTT:PbS QDs BHJ composite gave rise to the photocurrent, resulting in detectivities greater than 10^{12} Jones (cm Hz$^{1/2}$/W) over the wavelength region from 300 nm to 2000 nm under a low applied bias. Thus, our findings of the utilization of the PDDTT:PbS QDs BHJ composites and an "inverted" vertical photodiode without the incorporation of the transparent oxide electrodes provide a facile way to realize broadband PDs.

Conflicts of interest

We declare that we have no competing financial interest and all the financial support has been acknowledged in the manuscript.

Acknowledgements

References

1 A. Rogalski, Material considerations for third generation infrared photon detectors, *Infrared Phys. Technol.*, 2007, **50**, 240–252.

2 A. R. Jha, A. Jha and D. A. Jha, *IR technology: applications to electrooptics, photonic devices, and sensors*, Wiley, New York, 2000.

3 A. Rogalski, HgCdTe IR detector material: history, status and outlook, *Rep. Prog. Phys.*, 2005, **68**, 2267–2336.

4 C. Liu, K. Wang, P. Du, E. Wang, X. Gong and A. J. Heeger, Ultrasensitive solution-processed broad-band photodetectors using CH$_3$NH$_3$PbI$_3$ perovskite hybrids and PbS quantum dots as light harvesters, *Nanoscale*, 2015, **7**, 16460–16469.

5 X. Gong, M. Tong, Y. Xia, W. Cai, J. S. Moon, Y. Cao, G. Yu, C.-L. Shieh, B. Nilsson and A. J. Heeger, High-detectivity polymer photodetectors with spectral response from 300 nm to 1450 nm, *Science*, 2009, **325**, 1665–1667.

6 G. Konstantatos and E. H. Sargent, Nanostructured materials for photon detection, *Nat. Nanotechnol.*, 2010, **5**, 391–400.

7 I. Moreels, Y. Justo, B. D. Geyter, M. K. Haustraete and Z. Hens, Z. Size-tunable, bright, and stable PbS quantum dots: a surface chemistry study, *ACS Nano*, 2011, **5**, 2004–2012.

8 C. Giansante, I. Infante, E. Fabiano, R. Grisorio, G. P. Suranna and G. Gigli, "Darker-than-Black" PbS quantum dots: enhancing optical absorption of colloidal semiconductor nanocrystals *via* short conjugated ligands, *J. Am. Chem. Soc.*, 2015, **137**, 1875–1886.

9 K. Qiao, H. Deng, X. Yang, D. Dong, M. Li, L. Hu, H. Liu, H. Song and J. Tang, Spectra-selective PbS quantum dot infrared photodetectors, *Nanoscale*, 2016, **8**, 7137–7143.

10 F. W. Wise, Lead salt quantum dots: the limit of strong quantum confinement, *Acc. Chem. Res.*, 2000, **33**, 773–780.

11 F. Xia, T. Mueller and Y.-M. Lin, A. Valdes-Garcia, P. Avouris, Ultrafast graphene photodetector, *Nat. Nanotechnol.*, 2009, **4**, 839–843.

12 C.-H. Liu, Y.-C. Chang, T. B. Norris and Z. Zhong, Graphene photodetectors with ultra-broadband and high responsivity at room temperature, *Nat. Nanotechnol.*, 2014, **9**, 273–278.

13 K. Zhang, T. Zhang, G. Cheng, T. Li, S. Wang, W. Wei, X. Zhou, W. Yu, Y. Sun, P. Wang, D. Zhang, C. Zeng, X. Wang, W. Hu, H. J. Fan, G. Shen, X. Chen, X. Duan, K. Chang and N. Dai, Interlayer transition and IR photodetection in atomically thin type-II MoTe$_2$/MoS$_2$ van der Waals heterostructures, *ACS Nano*, 2016, **10**, 3852–3858.

14 Y. Xie, B. Zhang, S. Wang, D. Wang, A. Wang, Z. Wang, H. Yu, H. Zhang, Y. Chen, M. Zhao, B. Huang, L. Mei and J. Wang, Ultrabroadband MoS$_2$ photodetector with spectral response from 445 to 2717 nm, *Adv. Mater.*, 2017, **29**, 1605972.

15 N. S. Sariciftci, L. Smilowitz, A. J. Heeger and F. Wudl, Photoinduced electron transfer from a conducting polymer to buckminsterfullerene, *Science*, 1992, 1474–1476.

16 G. Yu, J. Gao, J. C. Hummelen, F. Wudl and A. J. Heeger, Polymer photovoltaic cells: Enhanced efficiencies *via* a network of internal donor-acceptor heterojunctions, *Science*, 1995, **270**, 1789–1791.

17 L. Zheng, T. Zhu, W. Xu, L. Liu, J. Zheng, X. Gong and F. Wudl, Solution-processed broadband polymer photodetectors with a spectral response of up to 2.5 μm by a low bandgap donor–acceptor conjugated copolymer, *J. Mater. Chem. C*, 2018, **6**, 3634–3641.

18 J. Han, J. Qi, X. Zheng, Y. Wang, L. Hu, C. Guo, Y. Wang, Y. Li, D. Ma, W. Qiao and Z. Y. Wang, Low-bandgap donor–acceptor polymers for photodetectors with photoresponsivity from 300 nm to 1600 nm, *J. Mater. Chem. C*, 2017, **5**, 159–165.

19 L. Hu, J. Han, W. Qiao, X. Zhou, C. Wang, D. Ma, Y. Li and Z. Y. Wang, Side-chain engineering in naphthalenediimide-based n-type polymers for high-performance all-polymer photodetectors, *Polym. Chem.*, 2018, **9**, 327–334.

20 L. Hu, W. Qiao, J. Han, X. Zhou, C. Wang, D. Ma, Z. Y. Wang and Y. Li, Naphthalene diimide–diketopyrrolopyrrole copolymers as non-fullerene acceptors for use in bulk-heterojunction all-polymer UV–NIR photodetectors, *Polym. Chem.*, 2017, **8**, 528–536.

21 X. Wang, L. Lv, L. Li, Y. Chen, K. Zhang, H. Chen, H. Dong, J. Huang, G. Shen, Z. Yang and H. Huang,

This journal is © The Royal Society of Chemistry 2022

J. Mater. Chem. C, 2022, **10**, 2783–2791 | **2789**

High-performance all-polymer photoresponse devices based on acceptor–acceptor conjugated polymers, *Adv. Funct. Mater.*, 2016, **26**, 6306–6315.

22 H. Wang, S. Xing, Y. Zheng, J. Kong, J. Yu and A. D. Taylor, Three-phase morphology evolution in sequentially solution-processed polymer photodetector: Toward low dark current and high photodetectivity, *ACS Appl. Mater. Interfaces*, 2018, **10**, 3856–3864.

23 X. Hu, K. Wang, C. Liu, T. Meng, Y. Dong, S. Liu, F. Huang, X. Gong and Y. Cao, High-detectivity inverted near-infrared polymer photodetectors using cross-linkable conjugated polyfluorene as an electron extraction layer, *J. Mater. Chem. C*, 2014, **2**, 9592–9598.

24 X. Liu, J. Zhou, J. Zheng, M. L. Becker and X. Gong, Water-soluble CdTe quantum dots as an anode interlayer for solution-processed near infrared polymer photodetectors, *Nanoscale*, 2013, **5**, 12474–12479.

25 L. Zhang, T. Yang, L. Shen, Y. Fang, L. Dang, N. Zhou, X. Guo, Z. Hong, Y. Yang, H. Wu, J. Huang and Y. Liang, Toward highly sensitive polymer photodetectors by molecular engineering, *Adv. Mater.*, 2015, **27**, 6496–6503.

26 W. Wang, F. Zhang, L. Li, M. Gao and B. Hu, Improved performance of photomultiplication polymer photodetectors by adjustment of P3HT molecular arrangement, *ACS Appl. Mater. Interfaces*, 2015, **7**, 22660–22668.

27 L. L. Li, F. J. Zhang, W. B. Wang, Q. S. An, J. Wang, Q. Q. Sun and M. Zhang, Trap-assisted photomultiplication polymer photodetectors obtaining an external quantum efficiency of 37 500%, *ACS Appl. Mater. Interfaces*, 2015, **7**(10), 5890–5897.

28 K. X. Yang, J. Wang, Z. J. Zhao, Z. J. Zhou, M. Liu, J. Zhang, Z. Q. He and F. J. Zhang, Smart strategy: transparent hole-transporting polymer as a regulator to optimize photomultiplication-type polymer photodetectors, *ACS Appl. Mater. Interfaces*, 2021, **13**, 21565.

29 Z. J. Zhao, M. Liu, K. X. Yang, C. Y. Xu, Y. X. Guan, X. L. Ma, J. Wang and F. J. Zhang, Highly sensitive narrowband photomultiplication-type organic photodetectors prepared by transfer-printed technology, *Adv. Funct. Mater.*, 2021, 2106009, DOI: 10.1002/adfm.202106009.

30 V. V. Diev, K. Hanson, J. D. Zimmerman, S. R. Forrest and M. E. Thompson, Fused pyrene-diporphyrins: shifting near-infrared absorption to 1.5 μm and beyond, *Angew. Chem., Int. Ed.*, 2010, **49**, 5523–5526.

31 E. Bundgaard and F. C. Krebs, Low band gap polymers for organic photovoltaics, *Sol. Energy Mater. Sol. Cells*, 2007, **91**, 954–985.

32 E. Perzon, F. Zhang, M. Andersson, W. Mammo, O. Inganäs and M. R. Andersson, A conjugated polymer for near-infrared optoelectronic applications, *Adv. Mater.*, 2007, **19**, 3308–3311.

33 G. Konstantatos, J. Clifford, L. Levina and E. H. Sargent, Sensitive solution-processed visible-wavelength photodetectors, *Nat. Photonics*, 2007, **1**, 531–534.

34 G. Konstantatos, I. Howard, A. Fischer, S. Hoogland, J. Clifford, E. Klem, L. Levina and E. H. Sargent, Ultrasensitive solution-cast quantum dot photodetectors, *Nature*, 2006, **442**, 180–183.

35 C. Liu, K. Wang, C. Yi, X. Shi, P. Du, A. W. Smith, A. Karim and X. Gong, Ultrasensitive solution-processed perovskite hybrid photodetectors, *J. Mater. Chem. C*, 2015, **3**, 6600–6606.

36 C. Liu, K. Wang, P. Du, E. Wang, X. Gong and A. J. Heeger, Ultrasensitive solution-processed broad-band photodetectors using $CH_3NH_3PbI_3$ perovskite hybrids and PbS quantum dots as light harvesters, *Nanoscale*, 2015, **7**, 16460–16469.

37 C. Liu, K. Wang, X. Gong and A. J. Heeger, Low bandgap semiconducting polymers for polymeric photovoltaics, *Chem. Soc. Rev.*, 2016, **45**, 4825–4846.

38 C. Liu, H. Peng, K. Wang, C. Wei, Z. Wang and X. Gong, PbS quantum dots-induced trap-assisted charge injection in perovskite photodetectors, *Nano Energy*, 2016, **30**, 27–35.

39 W. Xu, H. Peng, T. Zhu, C. Yi, L. Liu and X. Gong, A solution-processed near-infrared polymer: PbS quantum dot photo-detectors, *RSC Adv.*, 2017, **7**, 34633–34637.

40 L. Zheng, T. Zhu, W. Xu, J. Zheng, L. Liu and X. Gong, Ultrasensitive perovskite photodetectors by Co partially substituted hybrid perovskite, *ACS Sustainable Chem. Eng.*, 2018, **6**, 12055–12060.

41 T. Zhu, L. Zheng, X. Yao, L. Liu, F. Huang, Y. Cao and X. Gong, Ultrasensitive solution-processed broadband PbSe photodetectors through photomultiplication effect, *ACS Appl. Mater. Interfaces*, 2019, **11**, 9205–9212.

42 T. Zhu, Y. Yang, L. Zheng, L. Liu, M. L. Becker and X. Gong, Solution-processed flexible broadband photodetectors with solution-processed transparent polymeric electrode, *Adv. Funct. Mater.*, 2020, **30**, 1909487.

43 B. D. Gates, Flexible electronics, *Science*, 2009, **323**, 1566–1567.

44 D. Alemu, H.-Y. Wei, K.-C. Ho and C.-W. Chu, Highly conductive PEDOT:PSS electrode by simple film treatment with methanol for ITO-free polymer solar cells, *Energy Environ. Sci.*, 2012, **5**, 9662–9671.

45 X. Mei and J. Ouyang, Highly conductive and transparent single-walled carbon nanotube thin films fabricated by gel coating, *J. Mater. Chem.*, 2011, **21**, 17842–17849.

46 J. Du, S. Pei, L. Ma and H. M. Cheng, 25th Anniversary article: Carbon nanotube- and graphene-based transparent conductive films for optoelectronic devices, *Adv. Mater.*, 2014, **26**, 1958–1991.

47 Z. Yu, Q. Zhang, L. Li, Q. Chen, X. Niu, J. Liu and Q. Pei, Highly flexible silver nanowire electrodes for shape-memory polymer light-emitting diodes, *Adv. Mater.*, 2011, **23**, 664–668.

48 Y. Xia, K. Sun and J. Ouyang, Solution-processed metallic conducting polymer films as transparent electrode of optoelectronic devices, *Adv. Mater.*, 2012, **24**, 2436–2440.

49 Y. Xia, K. Sun and J. Ouyang, Highly conductive poly(3,4-ethylenedioxythiophene):poly(styrene sulfonate) films treated with an amphiphilic fluoro compound as the transparent electrode of polymer solar cells, *Energy Environ. Sci.*, 2012, **5**, 5325–5332.

50 M. Vosgueritchian, D. J. Lipomi and Z. Bao, Highly conductive and transparent PEDOT:PSS films with a

2790 | *J. Mater. Chem. C*, 2022, **10**, 2783–2791

This journal is © The Royal Society of Chemistry 2022

fluorosurfactant for stretchable and flexible transparent electrodes, *Adv. Funct. Mater.*, 2012, **22**, 421–428.

51 J. Ouyang, Solution-processed PEDOT:PSS films with conductivities as indium tin oxide through a treatment with mild and weak organic acids, *ACS Appl. Mater. Interfaces*, 2013, **5**, 13082–13088.

52 M. Sykora, A. Y. Koposov, J. A. McGuire, R. K. Schulze, O. Tretiak, J. M. Pietryga and V. I. Klimov, Effect of air exposure on surface properties, electronic structure, and carrier relaxation in PbSe nanocrystals, *ACS Nano*, 2010, **4**, 2021–2034.

53 D. K. Kim, Y. Lai, B. T. Diroll, C. B. Murray and C. R. Kagan, Flexible and low-voltage integrated circuits constructed from high-performance nanocrystal transistors, *Nat. Commun.*, 2012, **3**, 1216.

54 A. Nag, M. V. Kovalenko, J.-S. Lee, W. Liu, B. Spokoyny and D. V. Talapin, Metal-free inorganic ligands for colloidal nanocrystals: S^{2-}, HS^-, Se^{2-}, HSe^-, Te^{2-}, HTe^-, TeS_3^{2-}, OH^-, and NH^{2-} as surface ligands, *J. Am. Chem. Soc.*, 2011, **133**, 10612–10620.

55 A. T. Fafarman, W.-k. Koh, B. T. Diroll, D. K. Kim, D.-K. Ko, S. J. Oh, X. Ye, V. Doan-Nguyen, M. R. Crump, D. C. Reifsnyder, C. B. Murray and C. R. Kagan, Thiocyanate-capped nanocrystal colloids: vibrational reporter of surface chemistry and solution-based route to enhanced coupling in nanocrystal solids, *J. Am. Chem. Soc.*, 2011, **133**, 15753–15761.

56 T. Takagahara and K. Takeda, Theory of the quantum confinement effect on excitons in quantum dots of indirect-gap materials, *Phys. Rev. B: Condens. Matter Mater. Phys.*, 1992, **46**, 15578–15581.

57 H. Dong, H. Zhu, Q. Meng, X. Gong and W. Hu, Organic photoresponse materials and devices, *Chem. Soc. Rev.*, 2012, **41**, 1754–1808.

58 Y. Xia, L. Wang, X. Deng, D. Li, X. Zhu and Y. Cao, Photocurrent response wavelength up to 1.1 μm from photovoltaic cells based on narrow-band-gap conjugated polymer and fullerene derivative, *Appl. Phys. Lett.*, 2006, **89**, 081106.

59 T. Erb, U. Zhokhavets, G. Gobsch, S. Raleva, B. Stühn, P. Schilinsky, C. Waldauf and C. J. Brabec, Correlation between structural and optical properties of composite polymer/fullerene films for organic solar cells, *Adv. Funct. Mater.*, 2005, **15**, 1193–1196.

60 H. Krüger, E. Kemnitz, A. Hertwig and U. Beck, Transparent MgF_2-films by sol-gel coating: Synthesis and optical properties, *Thin Solid Films*, 2008, **516**, 4175–4177.

61 D. W. Steuerman, A. Garcia, M. Dante, R. Yang, J. P. Löfvander and T.-Q. Nguyen, Imaging the interfaces of conjugated polymer optoelectronic devices, *Adv. Mater.*, 2008, **20**, 528–534.

62 D. R. Rainer, C. Xu, P. M. Holmblad and D. W. Goodman, Pd, Cu, and Au particles on Al_2O_3 thin films: an infrared reflection absorption spectroscopy study of monometallic and bimetallic planar model supported catalysts, *J. Vac. Sci. Technol., A*, 1997, **15**, 1653–1662.

63 S. R. Cowan, A. Roy and A. J. Heeger, Recombination in polymer-fullerene bulk heterojunction solar cells, *Phys. Rev. B: Condens. Matter Mater. Phys.*, 2010, **82**, 245207.

64 J. L. Bredas and G. B. Street, Polarons, bipolarons, and solitons in conducting polymers, *Acc. Chem. Res.*, 1985, **18**, 309–315.

65 C. Deibel, T. Strobel and V. Dyakonov, Origin of the efficient polaron-pair dissociation in polymer-fullerene blends, *Phys. Rev. Lett.*, 2009, **103**, 036402.

66 S. M. Sze and K. K. Ng, *Physics of Semiconductor Devices*, John Wiley & Sons, Inc. 3rd edn, 2006.

67 Y. Wang, D. Yang, X. Zhou, D. Ma, A. Vadim, T. Ahamad and S. M. Alshehri, Perovskite/Polymer hybrid thin films for high external quantum efficiency photodetectors with wide spectral response from visible to near-infrared wavelengths, *Adv. Opt. Mater.*, 2017, **5**, 1700213.

68 W. Xu, Y. Guo, X. Zhang, L. Zheng, T. Zhu, D. Zhao, W. Hu and X. Gong, Room-temperature-operated ultrasensitive broadband photodetectors by perovskite incorporated with conjugated polymer and single-wall carbon nanotubes, *Adv. Funct. Mater.*, 2018, **28**, 1705541.

This journal is © The Royal Society of Chemistry 2022

J. Mater. Chem. C, 2022, **10**, 2783–2791 | **2791**